BEST AVAILABLE IMAGES

Defective images within this document are accurate representations of the original documents submitted by the applicant.

Defects in the images may include (but are not limited to):

- BLACK BORDERS
- TEXT CUT OFF AT TOP, BOTTOM OR SIDES
- FADED TEXT
- ILLEGIBLE TEXT
- SKEWED/SLANTED IMAGES
- COLORED PHOTOS
- BLACK OR VERY BLACK AND WHITE DARK PHOTOS
- GRAY SCALE DOCUMENTS

IMAGES ARE BEST AVAILABLE COPY.

As rescanning documents *will not* correct images, please do not report the images to the Image Problem Mailbox.

Derivation of Optical Constants of Metals from Thin-Film Measurements at Oblique Incidence

J. E. Nestell, Jr., and R. W. Christy

The reflectance R and transmittance T of thin absorbing films deposited on a transparent substrate are calculated for normal and oblique incidence, s and p polarization, and different film thicknesses. The results are presented as contours of constant R and T on the $\tilde{n}$ plane, where $\tilde{n}$ is the complex refractive index. The conditions for sensitive dependence of measured quantities on $\tilde{n}$ are examined. A computer-based method of finding $\tilde{n}$ from chosen combinations of measured R or T values is described. Oblique incidence measurements on thin films can give accurate results in some regions where other methods may be less sensitive. Accurate film-thickness values can be obtained from the optical measurements.

I. Introduction

Measurement of the reflectance and transmittance of a thin metal film is a common method of obtaining the optical constants n amd k of the metal,[1,2] In the past these measurements have usually been made at normal incidence. Our purpose is to describe some general procedures for analyzing measurements made at oblique incidence. Solution of the Maxwell-equation boundary-value problem with oblique incidence to obtain reflectance R and transmittance T in terms of the material constants n and k is straightforward,[3] but the resulting functions are very complicated. Thus the problem of inverting the functions to obtain n and k in terms of the measured R and T is difficult. This difficulty has presumably discouraged attempts to make much practical use of oblique incidence measurements, but we shall show how computer graphing and inversion techniques make feasible the analysis of thin-film measurements at any angle of incidence. In addition, a judicious choice of incident angle and polarization can cope with some troublesome regions of n-k space where normal incidence measurements are inaccurate.[4] Some of these results and conclusions have been obtained previously.[5,6]

We shall consider an isotropic, homogeneous metal, bounded by plane-parallel surfaces, without being concerned with the validity of these assumptions for real evaporated films.[1] We exclude from consideration monocrystalline films of anisotropic metals; this limitation is not of importance at present because experimentally it is very difficult to deposit single crystal layers, and because the theoretical analysis of the optical measurements would be inordinately complicated. Therefore the problem is, starting with equations for R and T in terms of n and k under these assumed conditions, first to choose suitable combinations of R and T for measurement and second to invert the equations to obtain values for n and k.

The predicted values of R and T depend not only on n and k according to electromagnetic theory under the assumed conditions, but also on the thickness of the thin film and on the wavelength, angle of incidence, and polarization of the incident light. The last three quantities are usually determined by the disposition of the measuring apparatus. The values of n and k are expected to depend on wavelength of the light (photon energy which excites the electronic transition), but not on polarization and angle of incidence (in the isotropic case) or on thickness, since n and k are material constants independent of the bounding surfaces. Therefore in order to find n and k as a function of wavelength, at each wavelength one must measure three values from among the following possibilities: (1) R at specified incident angles and polarizations, (2) T at specified incident angles and polarizations, and (3) film thickness. Varying the thickness is possible but inconvenient, since separate samples must be fabricated. (It also turns out to be less accurate,[4] except in certain regions of n-k space which are insensitive to other parameters.) Measurement of film thickness can be made by means that are independent of the R and T measurements, but the accuracy is usually not better than about ± 30 Å except under especially careful conditions.[7] One may therefore consider making three measurements from among possibilities for R and T (from which the thickness could then be de-

The authors are with Dartmouth College, Hanover, New Hampshire 03755.

Received 22 March 1971.

termined as well as n and k). We wish to choose optimum incident angle and polarization.

The limiting case of infinite thickness should be discussed separately, since it is often used experimentally, but of course the thickness disappears as a parameter and the transmittance is always zero. One can therefore make two measurements of R at different polarizations or incident angles on a bulk sample. An entirely different approach involves making a single measurement of R (usually at normal incidence) and using a Kramers-Kronig relation[8] to obtain the two quantities n and k. The latter approach has the advantage that it can be extended farther into the vacuum ultraviolet region where polarization of the incident light is difficult to control. It has the disadvantage that one *must* make measurements in this region, even in order to determine n and k only in the visible region. One must also make an assumption about the wavelength dependence of the reflectance outside the measurable range. Indeed, part of the interest in the techniques discussed here is to check the validity of such assumptions. Finally we mention the Drude (ellipsometry) method, in which one measures the relative amplitudes and phases shifts of the reflected polarized light instead of its intensity. (Bulk-sample techniques have been used to measure anisotropic effects in single crystals.[9])

We shall discuss the behavior of R and T under different conditions of polarization, incident angle, and film thickness, in order to facilitate a choice of the best combination of measurements on thin films. The choice depends on the examination of contours plotted in n-k space. This procedure has been used previously for infinite thickness[10] or for normal incidence.[4] Then we shall describe a computer-based iteration scheme that inverts the functions R and T to give the optical constants of the metal studied, and give an example to show how the scheme works. Comparisons will also be made with some bulk-sample methods in terms of the same criteria. We do not attempt a comprehensive evaluation of instrumental limitations of various methods,[7] which would give an over-all assessment of the best method for each circumstance.

II. Theoretical Formulas for R and T

A light wave is assumed incident from a dielectric medium 1 (e.g., air) onto the plane surface of metallic medium 2 at an angle of incidence θ_1 with the normal to the bounding surface. The back boundary of the metal layer is a plane-parallel interface with another dielectric medium 3 (e.g., a glass substrate). The reflectance and transmittance[11] of the metal layer are given by (tilde denotes a complex quantity)

$$R = |\tilde{r}|^2, \qquad T = (n_3/n_1)|\tilde{t}|^2,$$

where

$$\tilde{r} = [\tilde{r}_{12} + \tilde{r}_{23}\exp(i\tilde{\delta})]/[1 + \tilde{r}_{12}\tilde{r}_{23}\exp(i\tilde{\delta})],$$

$$\tilde{t} = [\tilde{t}_{12}\tilde{t}_{23}\exp(i\tilde{\delta}/2)]/[1 + \tilde{r}_{12}\tilde{r}_{23}\exp(i\tilde{\delta})].$$

The Fresnel coefficients for perpendicular polarization of the electric vector are

$$\tilde{r}_{12}{}^{s} = (n_1\cos\theta_1 - \tilde{n}_2\cos\tilde{\theta}_2)/(n_1\cos\theta_1 + \tilde{n}_2\cos\tilde{\theta}_2),$$

$$\tilde{t}_{12}{}^{s} = 2n_1\cos\theta_1/(n_1\cos\theta_1 + \tilde{n}_2\cos\tilde{\theta}_2),$$

and for parallel polarization,

$$\tilde{r}_{12}{}^{p} = (\tilde{n}_2\cos\theta_1 - n_1\cos\tilde{\theta}_2)/(\tilde{n}_2\cos\theta_1 + n_1\cos\tilde{\theta}_2),$$

$$\tilde{t}_{12}{}^{p} = 2n_1\cos\theta_1/(\tilde{n}_2\cos\theta_1 + n_1\cos\tilde{\theta}_2).$$

(The permeability of all three media is assumed equal to μ_0 for free space.)

$$\tilde{\delta} = 4\pi(d/\lambda)n_2\cos\tilde{\theta}_2,$$

where d is the film thickness and λ is the vacuum wavelength of the incident light. Similar expressions are obtained for $\tilde{r}_{23}$ and $\tilde{t}_{23}$ by permuting the subscripts; n_3 and θ_3 are real.

The angle θ_1 is the angle of incidence of the light wave and n_1 is the refractive index of medium 1. The complex angle $\tilde{\theta}_2$ is defined by Snell's law, $\tilde{n}_2\sin\tilde{\theta}_2 = n_1\sin\theta_1$; also $\tilde{n}_2 = n + ik$, where n and k are the optical constants of the metal that we wish to find. We make the definition

$$\tilde{n}_2\cos\tilde{\theta}_2 \equiv u + iv.$$

Then one finds[3]

$$u^2 = \tfrac{1}{2}\{(n^2 - k^2 - n_1{}^2\sin^2\theta_1) + [4n^2k^2 + (n^2 - k^2 - n_1{}^2\sin^2\theta_1)^2]^{\frac{1}{2}}\},$$

$$v^2 = \tfrac{1}{2}\{-(n^2 - k^2 - n_1{}^2\sin^2\theta_1) + [4n^2k^2 + (n^2 - k^2 - n_1{}^2\sin^2\theta_1)^2]^{\frac{1}{2}}\},$$

$$\cos\tilde{\theta}_2 = (u + iv)/(n + ik).$$

Finally,

$$\tilde{n}_3\cos\theta_3 = (n_3{}^2 - \tilde{n}_1{}^2\sin^2\theta_1)^{\frac{1}{2}}.$$

The above formulas for u and v appear somewhat simpler when expressed in terms of the complex dielectric constant $\tilde{\epsilon} = \epsilon_r + i\epsilon_i$, where $\tilde{\epsilon} = \tilde{n}^2$. In addition, $\tilde{\epsilon}$ is more directly related to the electron theory of the metal. Nevertheless, we present our discussion in terms of $\tilde{n}$. The mapping $\tilde{\epsilon} = \tilde{n}^2$ is a conformal mapping, and so all the conclusions that we draw below about the intersections of contours of constant R and constant T in the n-k plane would hold also in the ϵ_r-ϵ_i plane. The former has the advantage of magnifying the interesting region near the origin.

These formulas are sufficient to determine R and T in terms of n and k. In the application to metals we should note that the derivation from Maxwell's equations assumes *local* conductivity. If nonlocal effects are included, a longitudinal wave gives anomalous absorption of p-polarized light near the plasma frequency,[12,13] but this is normally very small. The ordinary transverse wave, excited by s-polarized light as well, is modified by the anomalous skin effect,[14-16] which gives larger anomalies in the infrared, especially if the electron reflection at the metal surface is diffuse. Apparently, however, the above formulas can be used

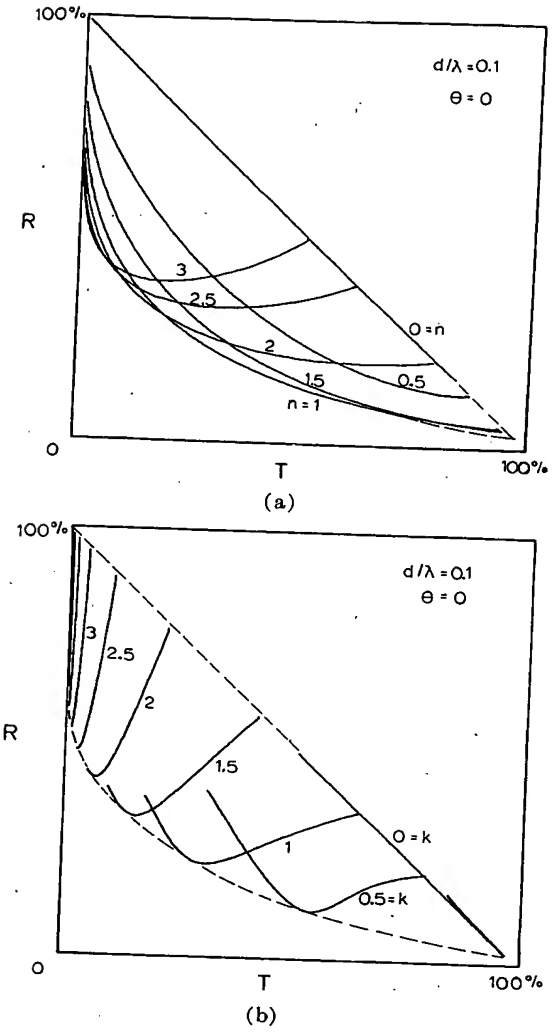

Fig. 1. Contours of const. n and k for normal incidence and $d/\lambda = 0.1$. (a) For each curve n has the value indicated and $0 \leq k \leq 4$. (b) For each curve k has the value indicated and $0 \leq n \leq 3$.

for the relation between the reflectance and transmittance and the optical constants, and the anomalous skin effect can be introduced afterwards as a modification in the classical Drude free-electron theory.[14]

III. Contours of R and T

Our main purpose is to be able to obtain experimental values of n and k from measurements of R and T. According to the formulas of Sec. II, R and T are single-valued functions of n and k, but it turns out that n and k are multiple-valued functions of R and T. Therefore it is essential to gain some insight into the functions before attempting to invert them. Erroneous solutions have been attributed to unawareness of this problem.[17] To illustrate this point, in Fig. 1 we plot contours of constant n and k in the R-T plane, for the case of normal incidence.[18] Only certain pairs of R and T values are physically possible. They must be below the line $R + T = 1$, and above the (common) envelope of the n and k contours (which depends on d/λ and θ). Two solutions for n and k are possible over much of the allowed area, for a particular R and T. If a larger range of n and k were considered, multiple solutions would occur over all of the allowed area.

For the purposes of seeing the behavior in the n-k plane and comparing our results with previous work, it is more valuable to look at contours of constant R and T in the n-k plane instead of Fig. 1. Unfortunately the functions cannot be inverted analytically, and so the contour-plotting routine is more costly in computer time. The functions R and T were calculated over a fine grid of points in a selected region of the n-k plane, for specified values of incident angle, polarization, and d/λ. If the calculated value of the function was within a chosen range of the nominal contour being plotted (chosen equal to an assumed error of 1% of full scale), the point was plotted before we went on to the next grid point. For the contours shown here, we have used $n_1 = 1$ (air), $n_3 = 1.46$ (quartz).

Results for normal incidence are redrawn in Fig. 2, for $d/\lambda = 0.1$. (The width of all the following contours is ± 0.005 for R and for $T > 0.1$, and ± 0.001 for $T \leq 0.1$.) The size of the shaded intersection suggests a nominal experimental error in the inferred n and k values due to uncertainties in the measured R and T values. The absolute error in n and k is large where (1) the two sets of contours are tangent to each other, or (2) one set of contours is widely spaced. The first feature is much more serious, since the region of overlap is far larger than the errors of measurement (especially for the n value, in this particular example).

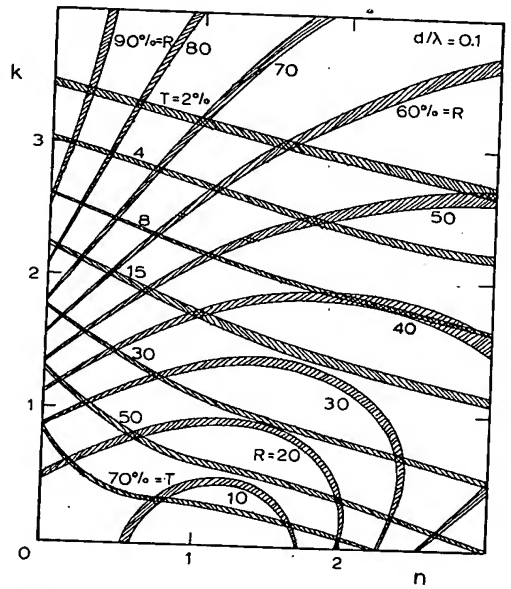

Fig. 2. Contours of const. R and T for normal incidence and $d/\lambda = 0.1$. The contour width indicates a nominal error of measurement, to show the uncertainty in the derived n and k values.

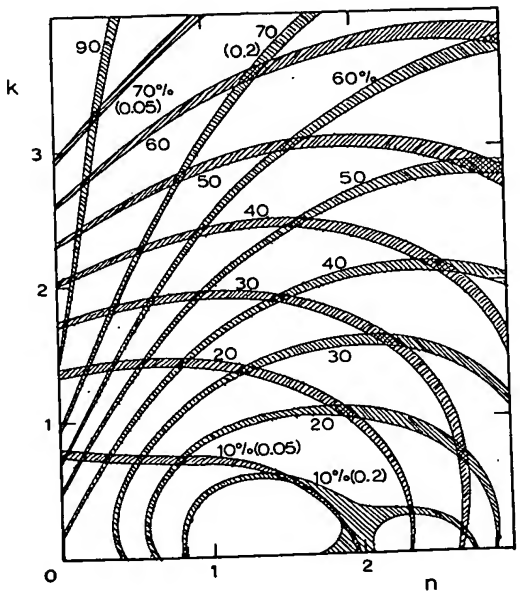

Fig. 3. Contours of const. R for normal incidence and $d/\lambda = 0.05$, 0.2.

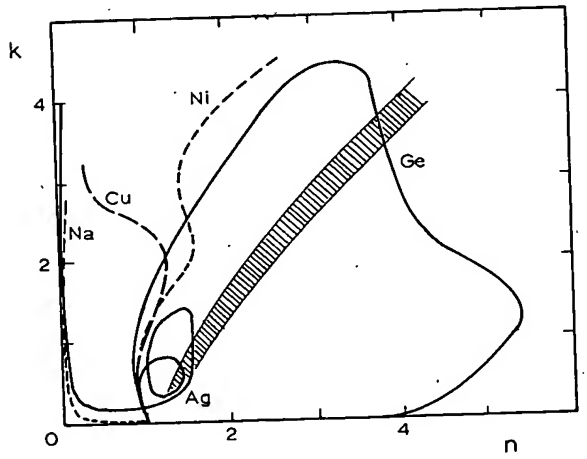

Fig. 4. Experimental values for some representative materials. The cross-hatched area is where the normal-incidence R and T contours are tangent for values of d/λ from 0.05 to 0.2.

The points of tangency lie near the line $k = n$, as has been observed previously.[4] Another related difficulty stems from the multiple intersections of a pair of contours. This ambiguity cannot be resolved without additional information.[5]

Normal incidence contours plotted for $d/\lambda = 0.05$ and 0.2 show the same general features as Fig. 2. The tangency of R and T contours still occurs near $k = n$, and multiple intersections occur. All the T contours for different d intersect at relatively small angles, as previously remarked,[4] giving large uncertainty in n. The R contours, however, intersect at angles greater than about 30° almost everywhere, and multiple intersections do not occur in the range considered. Figure 3 shows R contours for $d/\lambda = 0.05$ and 0.2. These may be useful, especially where the R and T contours are tangent, but we conclude (in agreement with Nilsson) that variation of film thickness probably does not give the most satisfactory method of analysis because of the uncertainties in thickness measurements.

To give some orientation toward the region of interest for real materials, in Fig. 4 we sketch on the same n-k plane values from the literature for some representative materials. Simple metals like Na avoid the difficult region of tangency, but others, notably Ag, enter it. Also the semiconductor Ge crosses it in the visible spectrum. Thus there is reason to consider the oblique incidence contours, even aside from their role in eliminating ambiguities and determining d, to be discussed below.

We begin with two general observations which will facilitate limiting our discussion to the interesting cases. First, at 60° angle of incidence a plot of R and T contours gives intersections that are qualitatively similar to Fig. 2 for normal incidence, for both s and p polarization. That is, the region of tangency shown in Fig. 4 and the multiple intersections still occur—in about the same location for s polarization and shifted roughly 0.5 to the right for p polarization. Therefore, we do not make a major gain by changing the angle for an R-T measurement. Second, the s polarization contours for both R and T are almost exactly parallel to the respective normal-incidence contours up to $d/\lambda = 0.2$, even at an incident angle as large as 75°. At a particular n and k, of course, the *value* of the reflectance is higher and the transmittance lower the larger the incident angle. Therefore, except for considerations of convenience and instrumental accuracy, the s-polarization case may be

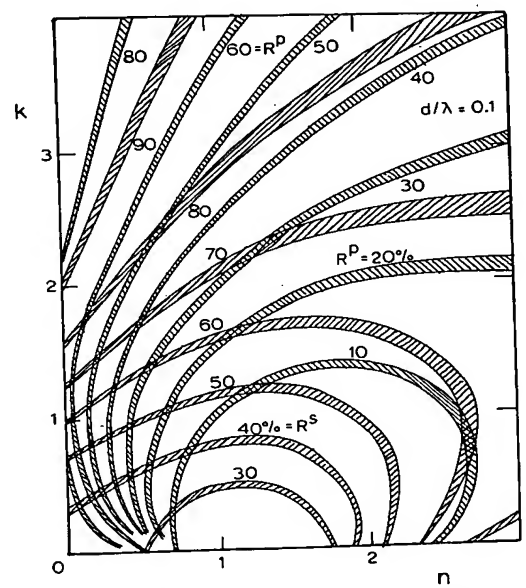

Fig. 5. Contours of const. R for s and p polarization with 60° incident angle and $d/\lambda = 0.1$.

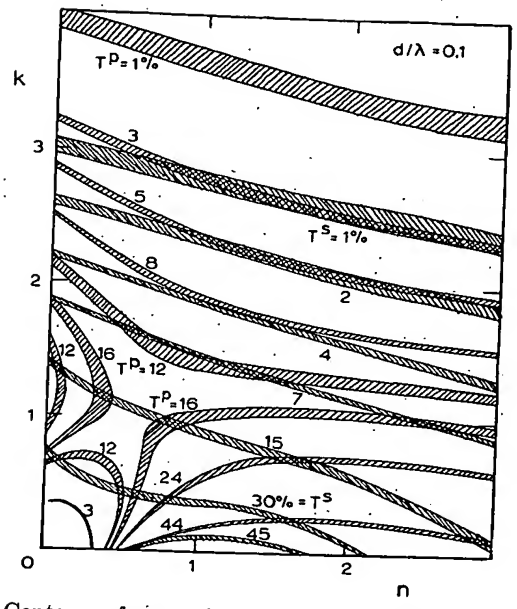

Fig. 6. Contours of const. T for s and p polarization with 60° incident angle and $d/\lambda = 0.1$.

equated to the normal-incidence case in our discussion.

The p-polarization contours, however, differ significantly in shape from the s-polarization (or normal incidence) contours. At 60° incident angle, these pairs of R contours (Fig. 5) and T contours (Fig. 6) intersect at useful angles in the region $n < 2$, $k < 2$, but outside this region they are approximately parallel. For 75° incidence, the useful region extends further. Also the useful region is larger the smaller d/λ is. (We shall allude to the latter point in connection with our later discussion of measurements on bulk samples.) Therefore the measurement of R or T at large angles on thin films can produce useful additional information in the range 1–6 eV for many materials.

Experimentally, when a spectrophotometer is used, measurements of T at various angles are especially easy. Thus we give an example[19] for the case of Ag at 4.7 eV, where a measurement of T at 60° with p polarization, in conjunction with normal-incidence R and T measurements, not only resolves the ambiguity between the two intersection points of the normal-incidence contours, but also permits a determination of the film thickness. The contours for these particular measured values are shown in Fig. 7. The resolution of the ambiguity is seen to be beyond the experimental error, even though the intersection angles are not large; the thickness determination is considered in the next section. This example illustrates the usefulness of the oblique-incidence measurement on a thin film.

IV. Solutions for n and k

Many methods have been developed[1,20,21] to determine the optical constants n and k from measured reflectance $\bar{R}$ and transmittance $\bar{T}$. Because the equations $R(n,k) = \bar{R}$ and $T(n,k) = \bar{T}$ cannot be solved analytically, even for normal incidence on thin films or oblique incidence on thick samples, graphical methods have been favored until recently. Similar methods could be used for this problem, but a large inventory of graphs would have to be produced and using them would be fairly tedious. We concluded that the best method is to use a small number of contour graphs to estimate rough values of n and k, and then to use these rough values as a starting point in a computer search routine.[22] The latter is relatively fast in terms of computer time.

The computer inversion technique to be described for oblique incidence is similar to ones previously developed[4–6,23] based on the Newton-Raphson method[24] of finding the intersection of contours. A procedure that requires the explicit calculation of partial derivatives of R and T with respect to n and k would be very tedious because of the complexity of the relations for oblique incidence. Our procedure circumvents this requirement.

To outline the method, at first we assume that the thickness d of the film is known by an independent measurement, and we let ψ and ϕ represent the two quantities that have been selected for measurement from among the possibilities for R and T at various angles and polarizations. One starts the procedure at some wavelength with a pair of values n_0,k_0 that are the best estimates of the desired intersection point in the n-k plane, obtained by inspection of the contours of Sec. III or by some other means. (In practice one could start with a wavelength corresponding to a d/λ for which contours are available. For successive steps in λ one can take n_0,k_0 to be the n,k found in the preceding step. Since, as we saw in the preceding section, two intersections may occur in certain regions of

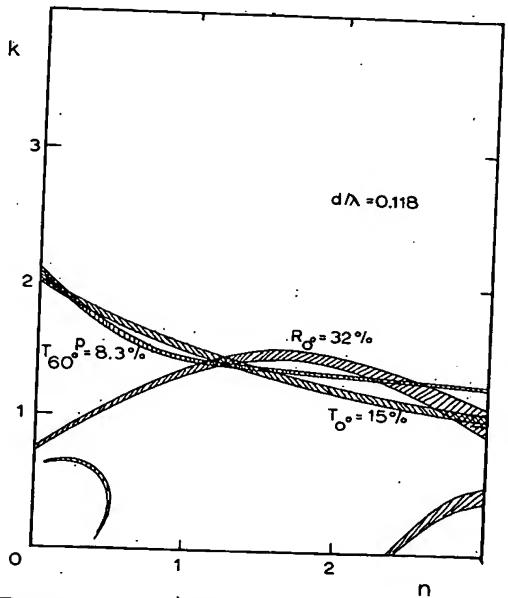

Fig. 7. Example of intersection of normal-incidence R and T contours with p-polarization T contour for 60° incident angle. $d/\lambda = 0.118$.

n-k space, the values of n_0,k_0 should be closer to the intersection desired.) One then calculates $\psi(n_0,k_0) = \psi_0$, $\phi(n_0,k_0) = \phi_0$, from the formulas of Sec. II, and the partial derivatives at n_0,k_0. Since it is inconvenient to calculate these partial derivatives explicitly, they will be determined by another method. Assuming for the moment that these derivatives are known, one next calculates the differences $\bar{\psi} - \psi_0$, $\bar{\phi} - \phi_0$, where $\bar{\psi}$ and $\bar{\phi}$ are the experimental values, and writes

$$(\Delta\psi)_0 \equiv \bar{\psi} - \psi_0 = \left(\frac{\partial\psi}{\partial n}\right)_0 \Delta n + \left(\frac{\partial\psi}{\partial k}\right)_0 \Delta k,$$

$$(\Delta\phi)_0 \equiv \bar{\phi} - \phi_0 = \left(\frac{\partial\phi}{\partial n}\right)_0 \Delta n + \left(\frac{\partial\phi}{\partial k}\right)_0 \Delta k.$$

These two linear equations in the unknowns $\Delta n,\Delta k$ can be solved easily. One then writes $n_1 = n_0 + \Delta n$, $k_1 = k_0 + \Delta k$ and inserts these new starting points into the procedure. After a small number of iterations, $\Delta\psi$ and $\Delta\phi$ approach zero and the procedure can be terminated with a printout of the corresponding n and k values.

At oblique incidence it is simpler to approximate the partial derivatives numerically than to calculate them analytically. A least-squares tangent approximation can be used, utilizing the matrix method of least-squares regression. One starts with the point (n_0,k_0) and considers a square of points symmetrically about it in the n-k plane, with corners at $(n_0 + \Delta n_0, k_0 + \Delta k_0)$, $(n_0 + \Delta n_0, k_0 - \Delta k_0)$, $(n_0 - \Delta n_0, k_0 + \Delta k_0)$, $(n_0 - \Delta n_0, k_0 - \Delta k_0)$. If Δn_0 and Δk_0 are sufficiently small, say of the order 0.01, then the functions $\psi(n,k)$, $\phi(n,k)$ are almost planar in this limited region and can be approximated by

$$\psi(n,k) \cong a_0 + a_1 n + a_2 k,$$

$$\phi(n,k) \cong b_0 + b_1 n + b_2 k,$$

where

$$a_1 = \left(\frac{\partial\psi}{\partial n}\right)_0, \quad a_2 = \left(\frac{\partial\psi}{\partial k}\right)_0, \quad b_1 = \left(\frac{\partial\phi}{\partial n}\right)_0, \quad b_2 = \left(\frac{\partial\phi}{\partial k}\right)_0.$$

One next constructs the following matrices:

$$\mathrm{X} \equiv \begin{pmatrix} 1 & (n_0 + \Delta n_0) & (k_0 + \Delta k_0) \\ 1 & (n_0 + \Delta n_0) & (k_0 - \Delta k_0) \\ 1 & (n_0 - \Delta n_0) & (k_0 + \Delta k_0) \\ 1 & (n_0 - \Delta n_0) & (k_0 - \Delta k_0) \end{pmatrix},$$

$$\Psi = \begin{pmatrix} \psi(n_0 + \Delta n_0, k_0 + \Delta k_0) \\ \psi(n_0 + \Delta n_0, k_0 - \Delta k_0) \\ \psi(n_0 - \Delta n_0, k_0 + \Delta k_0) \\ \psi(n_0 - \Delta n_0, k_0 - \Delta k_0) \end{pmatrix},$$

$$\Phi = \begin{pmatrix} \phi(n_0 + \Delta n_0, k_0 + \Delta k_0) \\ \phi(n_0 + \Delta n_0, k_0 - \Delta k_0) \\ \phi(n_0 - \Delta n_0, k_0 + \Delta k_0) \\ \phi(n_0 - \Delta n_0, k_0 - \Delta k_0) \end{pmatrix}.$$

From least-squares regression theory we have,[25] denoting the transpose of X by X^T,

$$\mathbf{a} = (\mathrm{X}^T\mathrm{X})^{-1}\mathrm{X}^T\Psi, \qquad \mathbf{b} = (\mathrm{X}^T\mathrm{X})^{-1}\mathrm{X}^T\Phi,$$

where

$$\mathbf{a} \equiv \begin{pmatrix} a_0 \\ a_1 \\ a_2 \end{pmatrix}, \qquad \mathbf{b} \equiv \begin{pmatrix} b_0 \\ b_1 \\ b_2 \end{pmatrix}$$

Reading a_1, a_2, b_1, b_2 from the vectors **a** and **b** gives the partial derivatives. This procedure is repeated at each iteration in the Newton-Raphson scheme. Our program usually requires three to five iterations for convergence of n and k to one part in 10^6. Tested against the normal-incidence examples given by Abelès and Thèye,[23] its results were exactly the same as theirs.

This procedure may be expanded to include a search for the film thickness d if that is not known.[6] The effect of d on the solution for n and k is illustrated in Fig. 8. (This figure shows, incidentally, that linear interpolation between sets of contours for different d/λ is usually satisfactory for a rough estimate of n and k.) The value of d/λ inserted into the two-parameter search routine affects the solution for n and k significantly, and if it is too far off, no intersection will be found at all in some cases. Measuring d directly with accuracy is difficult, especially for thinner films, although a standard interferometric measurement gives a suitable starting value for the following three-parameter search routine. The generalization of the procedure to include a search for d requires measurement of three quantities among the various R and T combinations, and an estimate of the starting point (n_0,k_0,d_0). The generalization[22] from two to three dimensions is straightforward, and so the details of the analysis are omitted.

Often the measurements are made at many different wavelengths on a single film. The three-parameter fits at different wavelengths will converge to different values

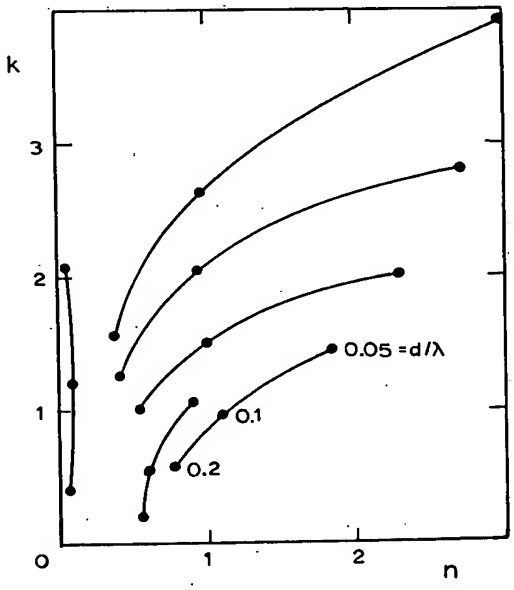

Fig. 8. Loci of the intersections of some particular normal-incidence R and T contours for d/λ values from 0.05 to 0.2.

of d because of experimental errors in the measurements, but the physical thickness of the film is actually the same at all the wavelengths. Therefore one should average the d values obtained at those wavelengths where the contour intersections provide accurate solutions, leaving out those near where tangencies or other inaccuracies occur. Then improved values of n and k are obtained by carrying out a new two-parameter fit using this average value of d together with the best pair of R and T values at each wavelength. For example,[19] in Ag for light between 0.5 and 6 eV a three-parameter fit gave d values which were in the range 310 ± 10 Å, except near the 4-eV plasma resonance and in the infrared where two of the three contours are nearly parallel. The unreliable regions can be recognized without reference to the contours by large deviations of d from the average or by failure of the three-parameter fit to converge at all. The error in the average d value can be much smaller than the scatter, perhaps 1 or 2 Å. This method has the additional advantage of giving automatically the (short-range) average thickness over the entire area of the film that is exposed to the light beam (assuming that the average thickness is constant over the illuminated area, which is greater for oblique than for normal incidence).

V. Comparison of Thin-Film and Bulk-Sample Methods

It is informative to look at some bulk-sample methods for determination of n and k in the same terms as our discussion of the thin-film possibilities. Such a comparison is necessarily incomplete, since considerations of the different instrumental limitations[7] are essential to an analysis of ultimate accuracy, but it is useful to put all these methods into the same perspective.

Most closely related to the thin-film calculations and methods are measurements of R on infinitely thick samples at two angles of incidence or two different polarizations.[26,27] For this case, $T = 0$ and $R = |\tilde{r}_{12}|^2$. We have already remarked that the s-polarization contours are parallel at all incident angles (except near the origin for infinite thickness), so that one can rely on a comparison between p polarization at a large angle with either s polarization or small incident angle. In Fig. 9 are shown the R contours for normal incidence and for p polarization at 60° incident angle, for infinite thickness. (This is the more useful comparison, because the s- and p-polarization contours at 60° become parallel near the origin for infinite thickness.) These may be compared with the thin-film contours of Fig. 5. The bulk contours intersect at small angles for $k > 2$. At 75° incident angle they can be used up to about $k = 4$, except for $n < 0.5$. Thus we conclude that a measurement of R at two incident angles or polarizations does not usually encounter the problem of ambiguous solutions, but it would yield greater accuracy with thinner samples,[5] leaving aside problems of sample preparation and thickness measurement. These measurements (especially for k values) are least reliable at large k and small n.[27]

For the Kramers-Kronig analysis, we consider $\tilde{r}_{12} \equiv r \exp(i\phi)$ in polar form, at normal incidence where $\tilde{r}_{12} = (\tilde{n} - 1)/(\tilde{n} + 1)$ for both s and p polarization. The normal-incidence reflectivity, $R = r^2$, is measured as a function of wavelength, and the phase ϕ is obtained from it by the integral dispersion relation

$$\phi(\omega) = -\frac{2\omega}{\pi}\int_0^\infty \frac{\ln r(\omega')d\omega'}{\omega'^2 - \omega^2},$$

or some variant of it.[28,29] (The same kind of analysis can also be applied to T measurements on thin films.[4]) Then n and k can be expressed explicitly in terms of r and ϕ:

$$n = (1 - r^2)/(1 + r^2 - 2r\cos\phi),$$

$$k = 2r\sin\phi/(1 + r^2 - 2r\cos\phi).$$

The contours r = const. and ϕ = const. are orthogonal trajectories of each other, since the function $\tilde{n}(\tilde{r}_{12})$ is analytic. Thus the problems of tangent contours and multiple intersections do not arise when this approach is used. In fact the contours are families of circles, because the function $\tilde{n}(\tilde{r}_{12})$ is a linear fractional transformation. In Fig. 10 the contours for R and ϕ are shown. The R contours are circles of radius $(P^2 - 1)^{\frac{1}{2}}$ centered at $n = P$, $k = 0$, where $P \equiv (1 + R)/(1 - R)$; the ϕ contours are circles of radius $(Q^2 + 1)^{\frac{1}{2}}$ centered at $n = 0$, $k = Q$, where $Q \equiv 1/\tan\phi$. From the spacing of the ϕ contours, one would conclude that the largest uncertainties are introduced in k at large k and small n (as in the preceding method). Consideration of the accuracy of the integral evaluation of ϕ is beyond the scope of our discussion, although it is important in practice.[30–32]

The Drude method depends on the comparison of $\tilde{r}_{12^s} \equiv r_s \exp(i\phi_s)$ and $\tilde{r}_{12^p} \equiv r_p \exp(i\phi_p)$ at oblique inci-

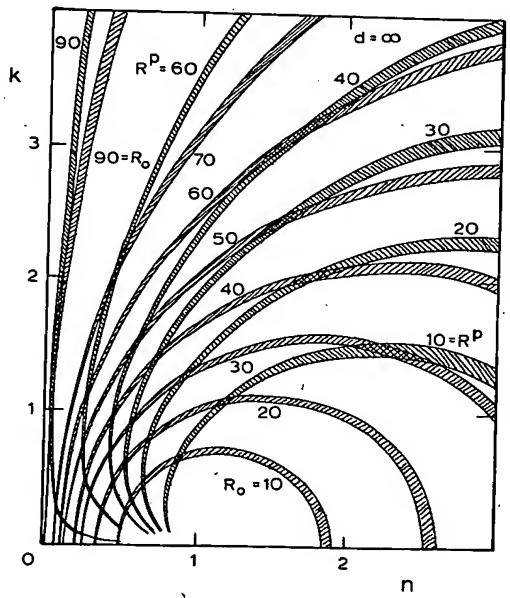

Fig. 9. Contours of const. R for normal incidence and p polarization at 60° incidence for infinite thickness.

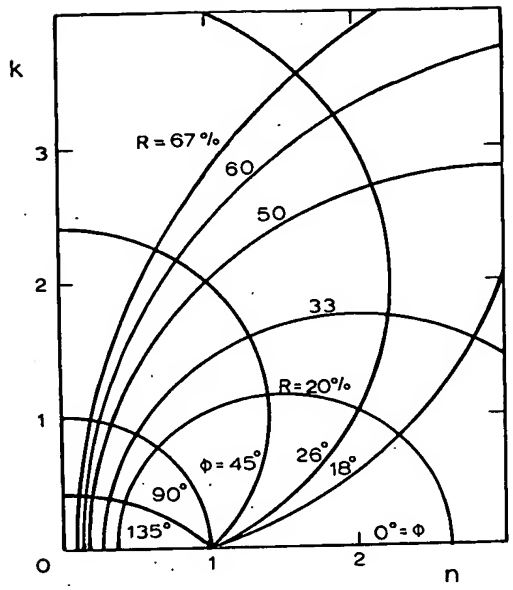

Fig. 10. Contours of const. R and const. phase ϕ for normal incidence and infinite thickness (Kramers-Kronig method).

dent angle. One measures ψ and Δ, where $\tilde{r}_{12}^{p}/\tilde{r}_{12}^{s} \equiv (\tan\psi)\exp(i\Delta)$, or $\tan\psi \equiv r_p/r_s$ and $\Delta \equiv \phi_p - \phi_s$. Experimentally ψ and Δ have usually been measured using polarizers and a quarter-wave plate or compensator, so that the method has been most used near the visible region of the wavelength spectrum. Again n and k can be expressed explicitly in terms of ψ, Δ, and θ_1 (the angle of incidence).[33] The contours for ψ and Δ are again orthogonal trajectories of each other because the relation to $\tilde{n}$ is analytic (although not linear fractional). They are shown in Fig. 11 for two different incident angles. The method must be used with large incident angles, since for small angles $\tan\psi \simeq 1$ and $\Delta \simeq \pi$ everywhere in the n-k plane except near $n = 1$, $k = 0$. (In this region smaller incident angles could be useful.) For instrumental reasons a value of Δ near $\pi/2$ is preferred,[34] subject to some refinements.[35] From Fig. 11 we see that satisfying this criterion demands appreciable changes in incident angle as n and k vary with wavelength, but that a relatively large incident angle is desirable for most of the n-k space region under consideration. The contour spacing suggests that also for this method the errors are greatest at large values of k, but with special care good accuracy has been achieved.[36]

Finally it should be mentioned that methods involving p polarization at large incident angle may be sensitive to the experimental accuracy of the incident angle. These include the bulk reflectivity and Drude methods. For example, the dependence on incident angle is shown in Fig. 12 for R^p at ∞ thickness, in the case $n = 1$, $k = 1$. If the polarizing angle for this n and k ($\sim$52°) is chosen, the problem is minimized, but at larger angles it becomes important. For thin films, the sensitivity of T with p polarization is also shown in Fig. 12. The angle dependence is not a serious problem at 60°.

VI. Conclusions

Our general conclusion is that thin-film measurements at oblique incidence can give accurate values of n and k in some regions of the n-k plane where other methods are subject to significant uncertainties. Because they are especially easy experimentally using a standard spectrophotometer in the 1–6-eV region, they may well be the method of choice in that wavelength range for easily evaporated materials.

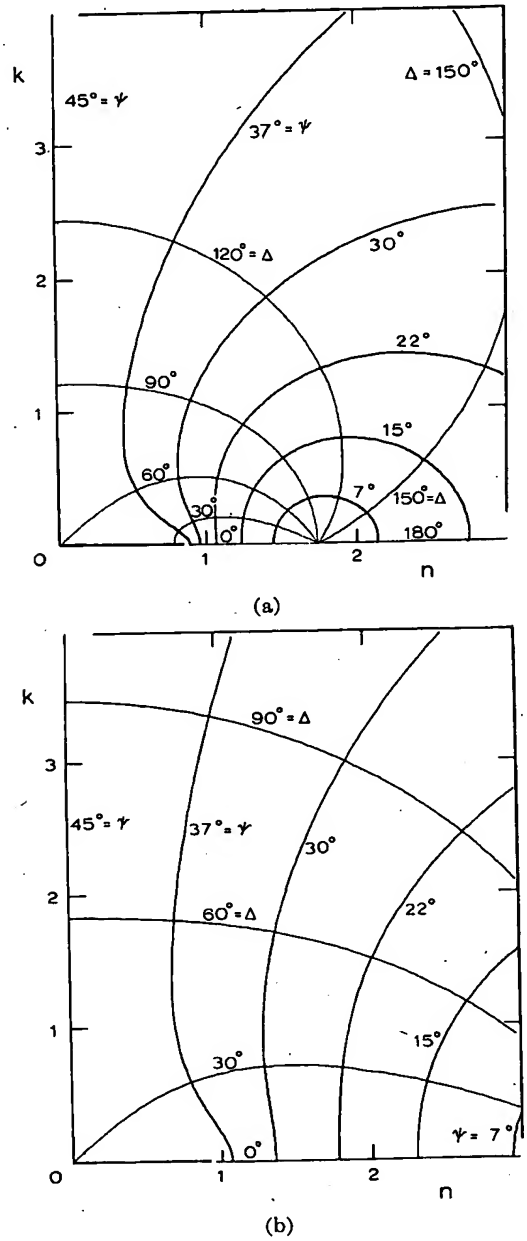

Fig. 11. Contours of const. ratio of amplitudes $\tan\psi$ and const. phase difference Δ for p and s polarization (Drude method). (a) 60° incidence; (b) 75° incidence.

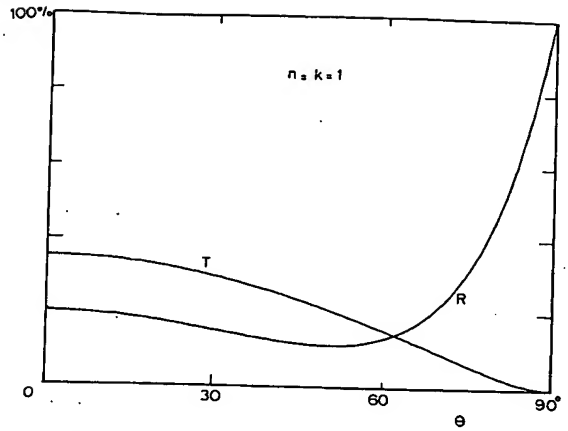

Fig. 12. Dependence on incident angle of R for infinite thickness and T for $d/\lambda = 0.1$, both with p polarization, in the case $n = k = 1$.

To determine n and k using thin films, the film thickness must also be determined. It can be obtained more accurately from three optical measurements, one of which may be p-polarized transmission, than by routine interferometric means. The third measurement could instead be R', the normal-incidence reflectance from the substrate–metal interface,[37] but R' is not very different from R and the procedure has not had much actual use. Therefore this improved accuracy is the main advantage of making thin-film measurements at oblique incidence. The procedure is also a convenient and accurate method for measuring the thickness of a thin film even aside from the optical constants.

The bulk methods considered here for comparison are inherently inaccurate in the region of large k and small n (especially for the k values), where by contrast the thin-film measurements give good accuracy. Some metals lie in this region at wavelengths in the near infrared. On the other hand, we have seen that normal-incidence thin-film measurements encounter difficulties in the region near $n = k$ but that these ambiguities can be resolved by measurements on the same film at oblique incidence with p polarization. Some metals lie in this region for visible wavelengths.

Problems of sample preparation have been left out of this consideration, but we may remark that the problems of surface smoothness and oxidation are especially important, and can be controlled in evaporated thin films. The question of the film structure may be raised; agreement of the n and k values obtained from films over the relatively wide range of thicknesses for which measurements are possible can allay doubts about this problem.

We are particularly grateful to P. B. Johnson for his important suggestions and assistance. We thank G. H. Zimmerman, III, for his help in computer programming.

This paper is based on part of a thesis submitted by J. E. Nestell, Jr., in partial fulfillment of the requirements for the A.M. degree.

References

1. O. S. Heavens, *Optical Properties of Thin Solid Films* (Butterworths, London, 1955).
2. A. Vašíček, *Optics of Thin Films* (North-Holland, Amsterdam, 1960).
3. See, for example, our discussion of this problem in Am. J. Phys. **39**, 313 (1971).
4. P. O. Nilsson, Appl. Opt. **7**, 435 (1968).
5. D. W. Juenker, J. Opt. Soc. Am. **55**, 295 (1965).
6. M.-G. Bouchard, in *Basic Problems in Thin Film Physics*, R. Niedermayer and H. Mayer, Eds. (Vandenhoeck & Ruprecht, Göttingen, 1966), p. 301.
7. H. E. Bennett and J. M. Bennett, in *Physics of Thin Films*, G. Hass and R. E. Thun, Eds. (Academic Press, New York, 1967), Vol. 4, p. 1.
8. T. S. Robinson, Proc. Phys. Soc. B **65**, 910 (1952).
9. A. P. Lenham, D. M. Treherne, and A. J. Woodall, in *Optical Properties and Electronic Structure of Metals and Alloys*, F. Abelès, Ed. (Wiley, New York, 1966), p. 40.
10. R. Tousey, J. Opt. Soc. Am. **29**, 235 (1939).
11. The transmittance is defined here as a ratio of power per unit area normal to the propagation direction, which differs in medium 1 and medium 3. Usually one measures the ratio of total power in a finite beam, which is $(\cos\theta_3/\cos\theta_1)T$. Experimentally, a correction must also be made in T and R for reflections at the back surface of the substrate.
12. F. Forstmann, Z. Physik **203**, 495 (1967).
13. R. Fuchs and K. L. Kliewer, Phys. Rev. **185**, 905 (1969).
14. R. B. Dingle, Physica **19**, 311, 729, 1187 (1953).
15. M.-L. Thèye, Phys. Lett. **25A**, 764 (1967).
16. K. L. Kliewer and R. Fuchs, Phys. Rev. B **2**, 2923 (1970).
17. D. Malé, cited in Ref. 1, p. 137.
18. These were plotted using a Timeshare Devices, Inc., C/P 701 plotter, by picking a value of n and stepping k (or vice versa).
19. P. B. Johnson and R. W. Christy, unpublished.
20. F. Abèles, in *Progress in Optics*, E. Wolf, Ed. (North-Holland, Amsterdam, 1963), Vol. 2, p. 249.
21. J. M. Bennett and M. J. Booty, Appl. Opt. **5**, 41 (1966).
22. Copies of the inversion programs in BASIC are available on request, as well as copies of the contours we have plotted.
23. F. Abelès and M.-L. Thèye, Surface Sci. **5**, 325 (1966).
24. H. Margenau and G. M. Murphy, *The Mathematics of Physics and Chemistry* (Van Nostrand, New York, 1947), p. 476.
25. N. Draper and H. Smith, *Applied Regression Analysis* (Wiley, New York, 1969).
26. S. P. F. Humphreys-Owen, Proc. Phys. Soc. **77**, 949 (1961).
27. W. R. Hunter, J. Opt. Soc. Am. **55**, 1197 (1965).
28. H. W. Bode, *Network Analysis and Feedback Amplifier Design* (Van Nostrand, New York, 1945), Chap. 14.
29. F. Stern, *Solid State Physics*, F. Seitz and D. Turnbull, Eds. (Academic, New York, 1963), Vol. 15, p. 299.
30. E. L. Green and L. Muldawer, Phys. Rev. B **2**, 330 (1970).
31. G. W. Rubloff, Phys. Rev. B **3**, 285 (1971).
32. D. L. Decker and J. L. Stanford, J. Opt. Soc. Am. **61**, 679A (1971).
33. M. Born and E. Wolf, *Principles of Optics* (Macmillan, New York, 1964), Sec. 13.2. Equations (12)–(14) contain misprints: the subscripts for perpendicular and parallel polarization should be interchanged.
34. P. Drude, Ann. Physik **39**, 504 (1890).
35. G. K. T. Conn and G. K. Eaton, J. Opt. Soc. Am. **44**, 546 (1954); J. R. Beattie and G. K. T. Conn, Philos. Mag. **46**, 223 (1955).
36. N. V. Smith, Phys. Rev. **183**, 634 (1969).
37. D. Malé, Compt. Rend. **230**, 1349 (1950).

Methods for absolute reflectance measurement of transmissive materials in the infrared

Leonard Hanssen and Simon Kaplan
Optical Technology Division
National Institute of Standards and Technology
Gaithersburg, Maryland

ABSTRACT

Four methods for the measurement of absolute reflectance are described and compared, with particular emphasis on application to transmissive materials such as windows and filters. Three of the methods, the 'V-W', 'V-N', and goniometer based methods, have been in use for a number of years. The fourth is an integrating sphere method. The sphere system is used for both specular and diffuse samples but achieves its greatest accuracy in the measurement of specular reflectance and transmittance.[1] A direct comparison of the sphere and goniometer methods is made on samples in the infrared spectral region.

1. INTRODUCTION

For absolute regular (specular) reflectance measurements, various methods including Strong's 'V-W',[2] 'V-N', and goniometer based methods are used.[3] These methods typically do not involve an integrating sphere. They involve an input beam, several directing mirrors, and the detector. Some subset of the mirrors, the sample, and the detector is manipulated via rotation and translation between 'sample' and 'reference' measurements. For the 'V-N' and goniometer methods, a simple ratio of the two results produces the absolute sample reflectance, while for the 'V-W' method, the square root is taken.[3,4]

The measurement of accurate absolute regular (specular) reflectance of samples is not an easy task. A number of potential problems can lead to measurement error. One that tends to dominate is alignment error. Source, sample and detector non-uniformity can increase the error caused by minute differences in the sample and reference measurement geometries. In addition, for transmissive samples, the measurement must include reflected light from the sample back surface. Because of the spatial displacement of the additional flux due to the extra path through the sample (and the potential deviation due to any wedging of the sample), the measurement error and consequently the uncertainty of the measurement results will increase, often significantly.

Integrating spheres can be used to substantially reduce the effects of alignment errors because they can present a large relatively uniform region for light detection in trade for reduced signal-to-noise. A recently developed integrating sphere method for absolute reflectance combines the benefits of local spatial uniformity in the sphere with a positioning system which arranges the beam, sample and sphere appropriately to obtain absolute results.[1]

The measurement geometries of the four absolute reflectance systems are described and discussed in Section 2. They are then qualitatively compared in Section 3, and a direct comparison of the sphere and goniometer systems using transmissive and opaque samples is described in Section 4. The conclusions are summarized in Section 5.

2. DESCRIPTION OF MEASUREMENT GEOMETRIES

The measurement of the absolute reflectance (or transmittance) of samples involves two separate measurements, generally sequential. This is true for both single beam and double beam instruments. In the discussions and figures to follow, these will be denoted as 'sample' and 'reference' measurements. The methods described in this paper are used with single wavelength, spectral and broadband instruments. For different spectral regions and different spectrophotometer designs, including filter, prism and grating monochromators, and Fourier transform (FT) instruments, details of the sources, beam geometries, optics, detectors, and operating environment may affect the specifics of the construction of a particular absolute reflectance accessory. These might include mirror coating and lens materials, angle of incidence, sample size, etc. However, the basic elements of the methods as described in this section remain independent of those details and specifics. In the following two Sections, specific implementation of two methods are presented for an infrared FT spectrophotometer system.

Part of the SPIE Conference on Optical Diagnostic Methods for Inorganic Transmissive Materials
San Diego, California • July 1998
SPIE Vol. 3425 • 0277-786X/98/$10.00

The 'V-W' method for absolute reflectance was first developed by Strong.[2] The basic arrangement is shown in Figure 1 for (a) sample 'W' and (b) reference 'V' measurements. In the sample measurement, two reflections take place on the sample, with an intervening reflection off a mirror. This requires a sample of sufficient size and spatial uniformity. For the reference measurement, the sample is removed and the mirror is repositioned by a rotation of 180° about the sample front surface as shown in Figure 1 (b). Even for opaque samples, careful alignment of the sample and mirror are critical to an accurate result.[5,6] For transmissive samples, the back surface reflections will be displaced according to the angle of incidence and the index of the material. The first order contribution from the first back surface reflection is shown by the dashed lines and from the second back surface reflection by the dotted line. In the V-W method, the second reflection off the sample will thus lead to a larger spread of the reflected light than for absolute methods with a single sample reflection. The use of an averaging sphere for detecting the output beam can be used to reduce sensitivity to alignment.

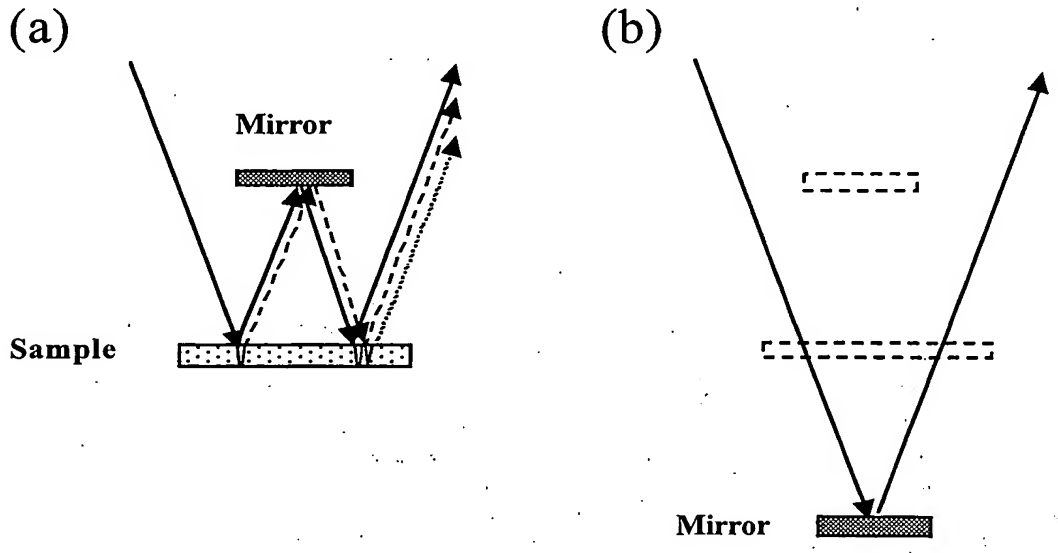

Figure 1. Schematic of Strong's V-W method for absolute reflectance measurement. The sample measurement geometry is shown in (a), in which two reflections take place off the sample and a mirror. For transmissive samples, the first order reflected components from the back surface are indicated as dashed and dotted arrows. For the reference measurement in (b), the sample is removed while the mirror flipped and translated. The beam path lengths and angles of incidence are maintained. The absolute reflectance value is obtained by taking the square root of the ratio of sample to reference measurements.

The 'V-N' method is shown in Figure 2. The sample, measured 'N' in (a), does not move for the reference measurement. Rather two mirrors are repositioned in the reference 'V' measurement (b). Mirror 1 is translated without rotation and mirror 2 is rotated without translation so that the beam travels the same path length and is incident on the mirrors at the same angles for both measurements. Only one reflection off the sample takes place and the absolute reflectance is obtained by a simple ratio of sample to reference measurement result. The additional beams coming from the back surface reflections are displaced from the first surface reflected beam. But the spread is less than in the 'V-W' case. As in the case of the 'V-W' method, accurate alignment is critical to high measurement accuracy. Also, an averaging sphere for the detector can be used to reduce sensitivity to alignment.

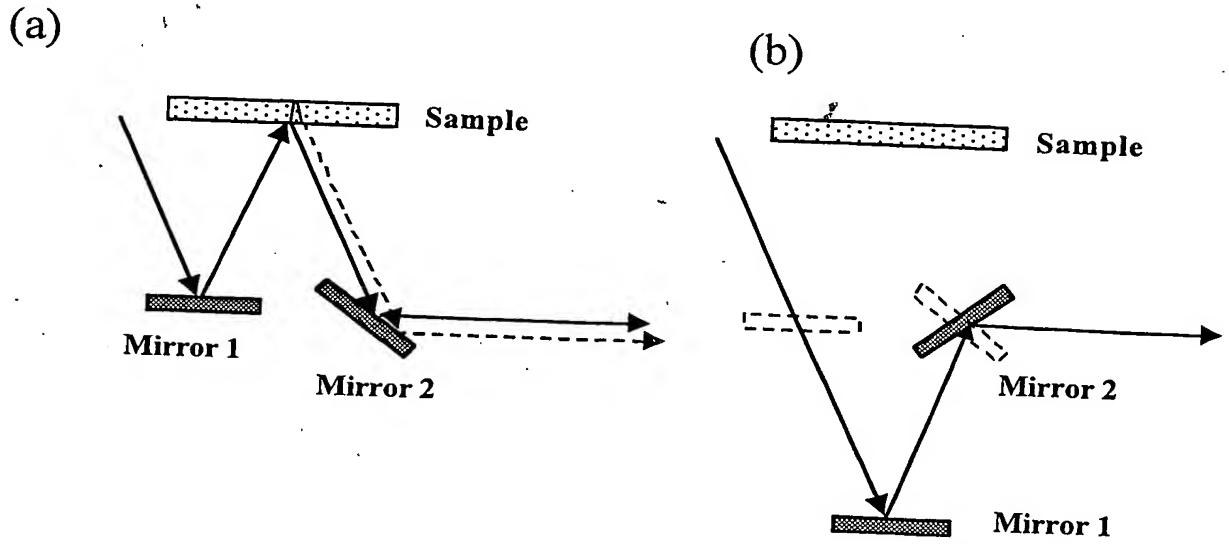

Figure 2. Schematic of V-N method for absolute reflectance measurement. The sample measurement geometry is shown in (a), in which reflections takes place off the sample and a pair of mirrors. The first order back surface reflected component is indicated with a dashed arrow. For the reference measurement in (b), mirror 1 is translated while mirror 2 is rotated. The beam path lengths and angles of incidence are maintained. The absolute reflectance value is the ratio of sample and reference measurements.

The goniometer method for absolute reflectance, shown in Figure 3, is the most basic of those discussed. The only components moved are the sample and detector (although variations exist with mirrors included). From the sample measurement arrangement shown in Figure 3 (a), the sample is moved out of the beam path and the detector is rotated about the sample center to intercept the beam directly in the reference measurement (b). In most designs this method requires more space than the other methods. However, it also offers more capabilities than the other methods. Specifically, with the addition of rotation of the sample about its own front surface, the goniometer can be used to measure reflectance at almost any angle. The range of angles is generally only limited near 0° and 90° by the beam geometry and physical size of the sample and detector. The alignment sensitivity for the goniometer method is similar to the 'V-N' method, and is reduced with the use of an averaging sphere for the detector.

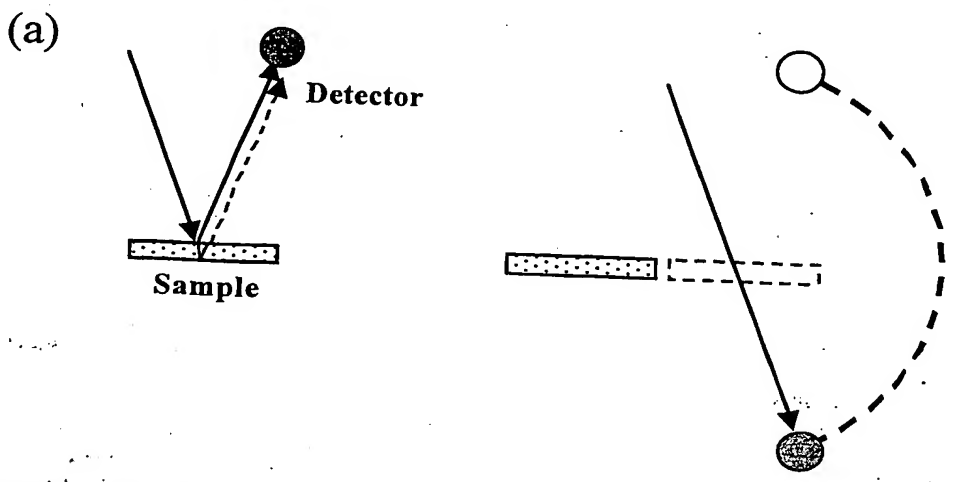

Figure 3. Schematic of goniometer based method for absolute reflectance measurement. The sample measurement is shown in (a), in which reflection off the sample takes place. The first order back surface reflected component is indicated with a

dashed arrow. For the reference measurement in (b), the sample is removed and the detector is rotated about an axis centered on the sample. The absolute reflectance value is the ratio of sample and reference measurements.

The fourth absolute reflectance method uses an integrating sphere as shown in Figure 4 and is detailed in Reference 1. The sample and reference measurement geometries in (a) and (b), respectively, are shown in top views. The specifics of the locations of the parts of the sphere are important only to the extent that symmetry is preserved between sample and reference measurements.[1] The input and reflected beams, and the sample, reference and entrance port centers, all lie in the plane containing the circular cross-section of the sphere shown in the figure. The detector is mounted on the top of the sphere and has a field of view (FOV) on the bottom of the sphere. The baffle is used to block the sample and reference from the FOV, and is located below the plane of the input and reflected beams. The sphere interior is coated with a high reflectance diffuser that acts to uniformly distribute light within the sphere. Besides the reflection off the sample, the only difference between the sample and reference measurements is the region of the sphere wall where the beams first hit. These are the 'specular' and 'reference' regions shown in Figure 4 (a) and (b), respectively, which are symmetrically placed on opposite sides of the entrance port. For the infrared sphere discussed in the following section, the ratio of the responsivity of these two regions to incident light is very close to 1.[7]

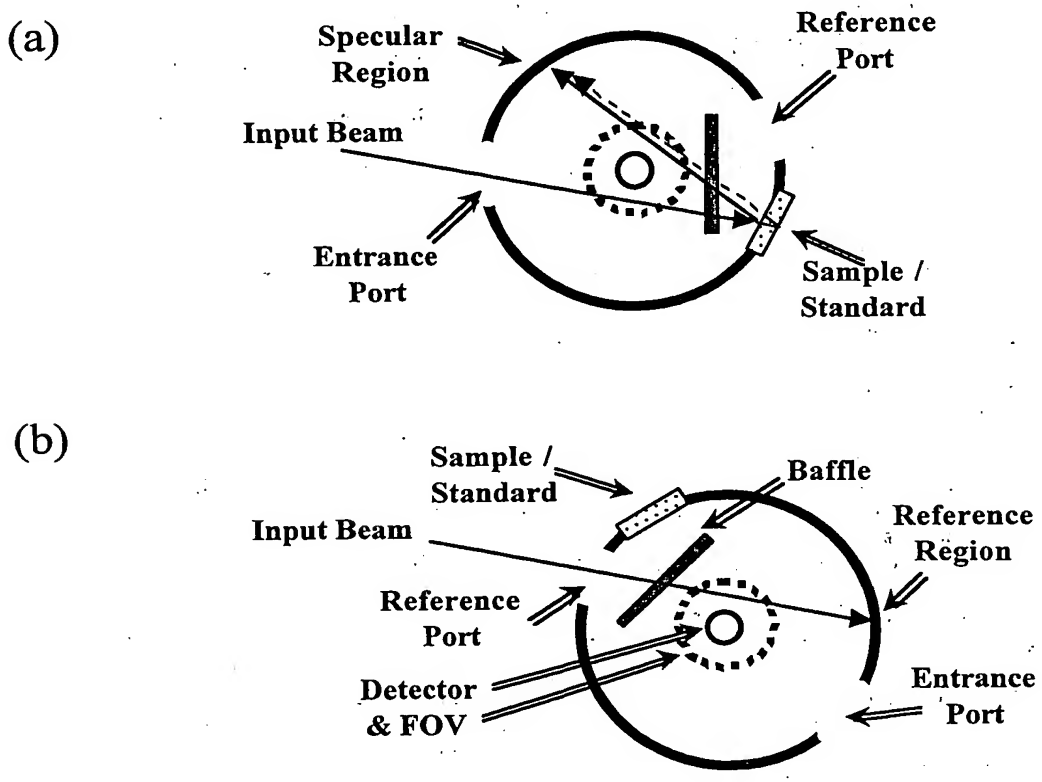

Figure 4. Schematic of integrating sphere based method for absolute reflectance measurement. Both (a) and (b) are top views. The sample measurement is shown in (a), in which reflection off the sample takes place. The first order back surface reflected component is indicated with a dashed arrow. For the reference measurement in (b), the sphere is rotated twice: first about the sample port and second about the sphere center. The baffle, detector and detector FOV are only labeled in (b). The baffle is positioned below the plane of the input and reflected beams. The absolute reflectance value is the ratio of the sample and reference measurements.

The additional light coming from the back surface reflections of the sample are displaced from the first surface reflected beam, but are all collected by the sphere with nearly equal efficiency. Because of the large area and solid angle of the uniform collecting area of the integrating sphere, transmissive samples can be accurately measured. In addition, other attributes of the sample such as surface flatness and wedge angle between the front and back surfaces, which can lead to large errors in other systems (which are sensitive to alignment), have very little effect on the sphere measurement accuracy.

A significant difference between the sphere method and the others described in this section is that the sphere has hemispherical collection. However, for samples that do not scatter, all four methods described should produce the same reflectance result. For samples that do scatter, the results will differ depending on the specifics of the beam geometries of the implementations of the other three methods (i.e. solid angles of incidence and measurement). More importantly, as discussed further in the Section 3, for samples with scatter only the sphere system can provide meaningful results.

3. QUALITATIVE COMPARISON OF METHODS

Some of the relative advantages and disadvantages of the four methods for absolute reflectance measurement of transmissive samples becomes apparent in the description of the geometries in Section 2. An overview of the advantages and disadvantages of the four methods is given in Table 1 at the end of this section.

Two advantages of the integrating sphere method are the insensitivity to alignment and the factors affecting alignment, as well as an ability to measure sample scattered light (away from the specular direction). As noted in Section 2, factors including sample thickness, flatness, parallelism, and alignment are all important for the non-sphere methods and can result in significant errors in the determination of the sample reflectance. For the sphere method all of these factors will result in small displacements of the light incident on the sphere wall. The small displacements will lead to minimal variations in detected signal due to the excellent local spatial uniformity of good sphere designs.[8] For the other methods, incorporation of an integrating sphere in front of the detector can be used to reduce sensitivities to alignment factors. However, only a sphere method design can be used for sorting out sample scattered light.

Because of the low throughput of integrating spheres, especially in the infrared, the measurement of very low reflectance in the sphere method is limited by a reduced signal-to-noise ratio, as compared to the 'V-N' and goniometer methods. For the infrared spectral range, the viability of the integrating sphere method is dependent on the use of FT spectrometers. Without the signal-to-noise advantages of FT instruments, the noise component of the uncertainty would be too large for most purposes. Hence the sphere method is probably not feasible for use with most infrared monochromator systems.

It is often not clear whether the sample may be scattering light to some degree in some spectral region. Verification of the absence of scatter is as important as accurately measuring the scatter that may exist.[9] The integrating sphere can be used to perform both functions. This can be done for both reflectance and transmittance. For the measurement of scatter in reflectance, a compensating wedge can be used so that the specularly reflected beam in Figure 4 (a) exits the sphere through the entrance port.[7] For the measurement of scatter in transmittance, the sphere can be rotated about the sample from its normal transmittance position so that the specularly transmitted beam exits the sphere through the entrance port.

Because of the pair of reflections off the sample in the 'V-W' method, high reflectance samples can, in principle, be measured more accurately than with other methods. When the square root of the result is taken, the corresponding relative uncertainty is halved. But for low reflectance samples, the sample measurement signal is lower by an amount equal to the reflectance and the relative uncertainty correspondingly greater than for single reflection absolute methods.

One way to evaluate the accuracy of the measurement of the reflectance of transmissive samples is to also measure the transmittance, preferably in the same geometry. The additional transmittance information can be used to give the absorptance of the sample through flux conservation. And for spectral regions where no absorption is expected the 'absorptance' determined from the transmittance and reflectance becomes an indication of the size of the errors in the measurement. The sample mount must be designed to allow the transmitted beam to pass unobstructed behind the sample (and properly dealt with in the reflectance measurement case).

An example of this concept is shown in Figures 5 and 6. The results were obtained using the infrared integrating sphere system described in Section 4 set up with a FT spectrophotometer.[10] The absolute reflectance and transmittance of a 0.5 mm thick, 25 mm diameter silicon window were measured over a broad spectral range, of which Figure 5 shows the results for the 2 μm to 5 μm range, where minimal absorption is expected. Also plotted are the calculated transmittance and

reflectance obtained from handbook values of the index of refraction.[11] The local structure in both spectra is the result of noise associated with the measurement made at 4 cm^{-1} resolution.

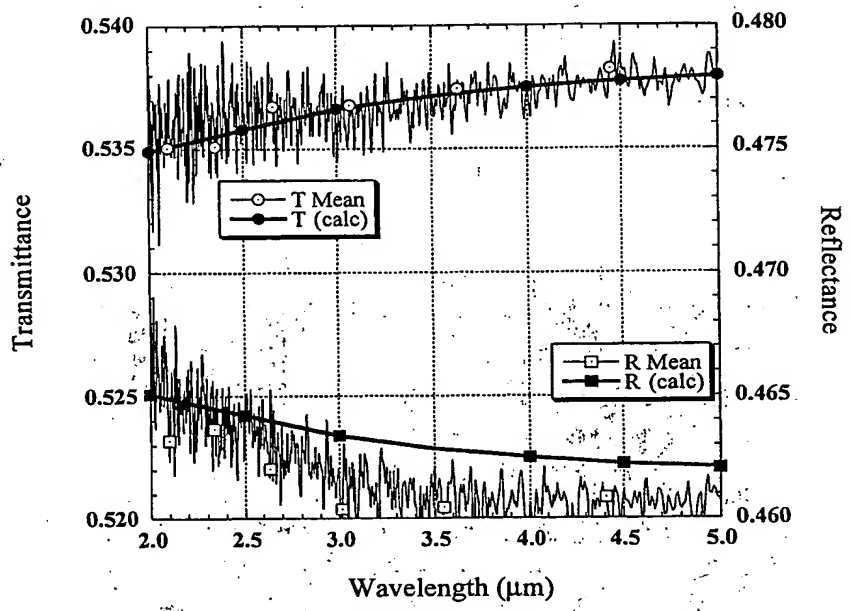

Figure 5. Absolute reflectance and transmittance of silicon window sample, as measured by the infrared integrating sphere system, and compared with calculated values using handbook n and k values.[10]

The absorptance determined from the reflectance and transmittance experimental data is plotted in Figure 6. For the spectral range of measurement, no absorptance should be seen. Hence the deviation from 0 absorptance is a gauge of the measurement error of the reflectance and transmittance. The level of ±0.002 in Figure 6 (ignoring the noise) is a reasonable estimate of the uncertainty of both the reflectance and transmittance measurements. Based only on these results this conclusion might be unwarranted, since conceivably errors in the two measurements could be of opposite sign and tend to cancel. However, numerous IR materials have been examined using the sphere system with reflectance values ranging up to 0.998 and down to 0.05 and corresponding transmittance values down to 0.002 and up to 0.95. The results of all of these measurements have been consistent with a maximum cumulative error in the range of ±0.003.

Thus the transmittance measurement result can be used to indirectly evaluate the accuracy of the reflectance result for transmissive samples. In principle designs incorporating transmittance capability are feasible for all four methods. Although not commonly found on 'V-W' accessories, transmittance measurement in the same setup is possible. The sample transmittance measurement can be made by translating the sample from its position in Figure 1 (a) so that the sample's edge is lined up vertically with the center of the mirror and the mirror moved to its position in Figure 1 (b). Then the input beam can pass through the sample and the mirror reflected beam in Figure 1 (b) can clear the sample's edge.

The 'V-N' geometry shown in Figure 2 does not accommodate a modification for transmittance measurement. However a hybrid design which incorporates features of the 'V-W' method can. The hybrid design sample measurement consists of that shown in Figure 2 (a), except with the sample and mirror 1 interchanged. The reference measurement is performed with mirror 2 rotated as in Figure 2 (b), but with mirror 1 relocated and the sample removed as in the 'V-W' case. In the hybrid reference measurement geometry, the sample transmittance can be measured by leaving the sample in position.

For the goniometer method, the transmittance measurement geometry is achieved by translating the sample back into place in the reference geometry shown in Figure 3 (b). For the sphere method, the transmittance measurement geometry is achieved by a pair of rotations placing the sample in the beam path of Figure 4 (b). This results in beam incidence on the same specular region as in the reflectance case.

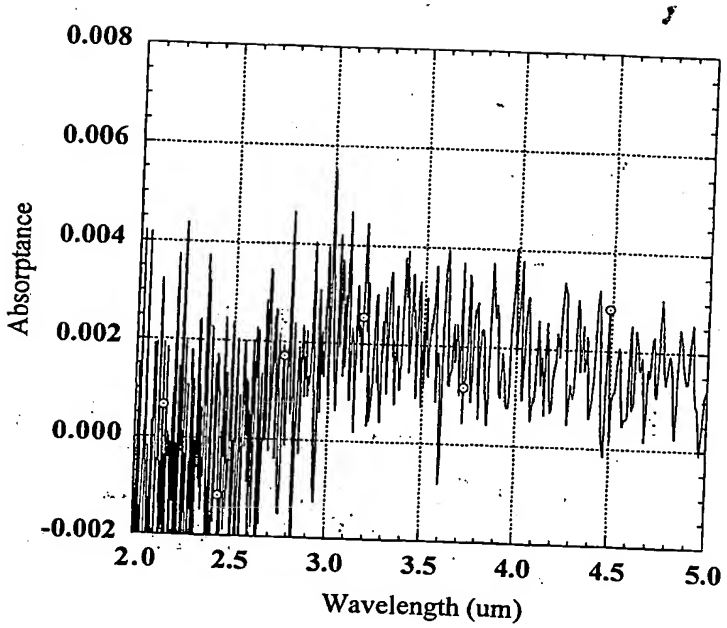

Figure 6. Absorptance calculated from the transmittance and reflectance data shown in Figure 5. In this spectral range the absorptance is silicon should be zero.[8] The absorptance values shown in this figure can be considered an indication of the accumulated errors in the measurement and thus a direct evaluation of the uncertainty of the transmittance and reflectance measurements.

In Table 1 the four absolute methods are compared in terms of a summary of their relative advantages denoted by a '+', and disadvantages denoted by a '-', whereas a '*' denotes feasibility with appropriate design modifications.

Table 1. Qualitative Comparison of Absolute Measurement Methods for Transmissive Samples

	V-W	V-N	Goniometer	Sphere
Accuracy at high reflectance	+	x	x	x
Accuracy at low reflectance	-	x	x	-
Requires larger uniform sample	-	x	x	x
Variable angle capability	x	x	+	x
Sensitive to sample flatness	-	-	-	+
Sensitive to sample parallelism	-	-	-	+
Sensitive to sample thickness	-	-	-	+
Sensitive to sample alignment	-	-	-	+
Can sort out scattered light from the sample	-	-	-	+
Sensitive to scattered light in the input beam	x	x	x	-
Transmittance capability in same geometry	*	*	+	+

4. DIRECT COMPARISON OF GONIOMETER AND SPHERE METHODS

Two methods for absolute reflectance described in this paper have been implemented on a FT spectrophotometer for near and mid IR operation (1 μm to 19 μm).[9] These are the integrating sphere and goniometer methods described in Sections 2 and 3. They are shown in photograph form in Figures 7 and 8.

The integrating sphere system shown in Figure 7 has been designed and constructed for absolute reflectance measurement of both diffuse and specular samples. The sphere is 15 cm in diameter with an entrance port of 33 mm diameter and sample and reference ports of 22 mm diameter. Baffles inside the sphere shade the sample and reference ports from the detector port on the top, and the detector FOV on the bottom, of the sphere. The inside wall of the sphere is coated with a nearly Lambertian diffuser that has a directional hemispherical (diffuse) reflectance of 0.9 for the infrared spectral range (plasma sprayed metal over-coated with gold). The IR beam from the FT Spectrophotometer is focused onto the sample at an incident angle of 8° and an f/5 cone. Spot sizes on the sample can be adjusted as required.

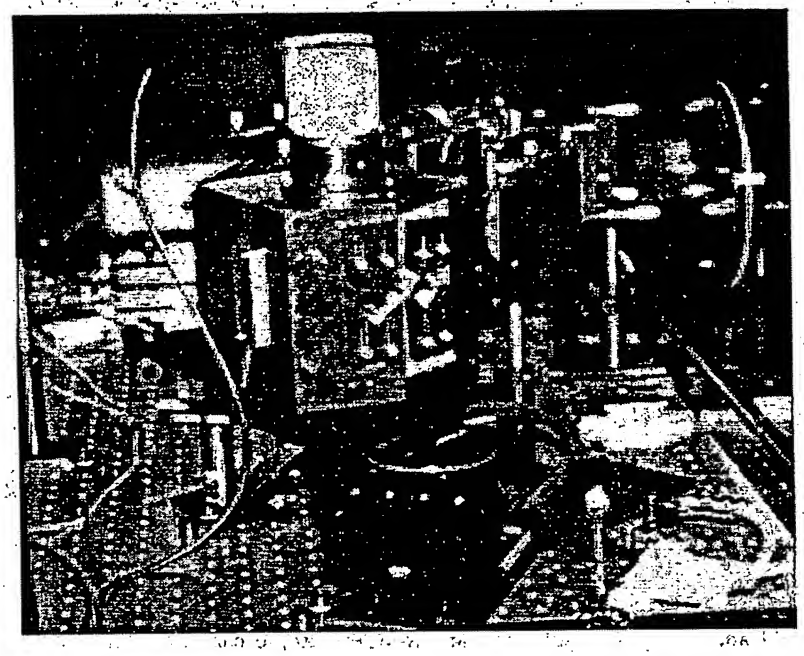

Figure 7. Rear view of infrared integrating sphere system for absolute reflectance and transmittance. The sample and reference ports are framed above and below by adjustable holders designed for use with transmissive samples. The dewar of the MCT detector can be seen at the top of the sphere. A pair of motorized rotation stages is located underneath the sphere for orienting it to the various positions for transmittance, reflectance, reference and other measurements.

An Hg:Cd:Te detector with nonimaging concentrator optics is mounted on the top of the sphere shown in Figure 7.[12] The entrance port for the input beam in reflectance mode is located on the back of the sphere in this photograph. The sample and reference ports can be seen in the foreground, with adjacent adjustable holders. These are designed to avoid obstruction to the sample transmitted light in the reflectance mode and to the input beam in the transmittance mode. Below the sphere are two rotation stages. The bottom stage has its axis of rotation centered on the input beam focus. The top stage holds the integrating sphere centered on its rotation axis and is mounted on the bottom stage off center. The top stage is used to select which sphere port is placed at the beam focus, and the bottom stage is used to vary the incidence angle of the beam on the selected port (from 0° to 360°). Hence reflected light can be measured in the orientation shown in Figure 7, while transmitted light can be measured with a 154° rotation of the bottom stage. Details of the sphere design and performance beyond those presented here can be found in References 1, 7 and 12.

The goniometer system shown in Figure 8 has been developed for a variety of tasks including variable reflectance and transmittance, polarimetry and ellipsometry. All the major components of the system are visible i photograph of the goniometer system in the reflectance measurement setup. The beam path follows along two optical that hold the input and output optics. Linear polarizers and retarders are mounted on a pair of rotation stages on each The fixed input beam (which originates from the FT) is brought from the back center in the photograph to the center c goniometer onto the sample, mounted in an optical access cryostat. The movable output rail also holds the detector focussing mirror at its end (at the left edge of the photograph). The output rail is mounted on a large rotation table, whi gear-driven by a stepper motor located at the back (to the right of the cryostat). The cryostat and a room temperature sa holder mounted on the optical table can be translated, rotated and tilted for alignment and defining the input beam angle.

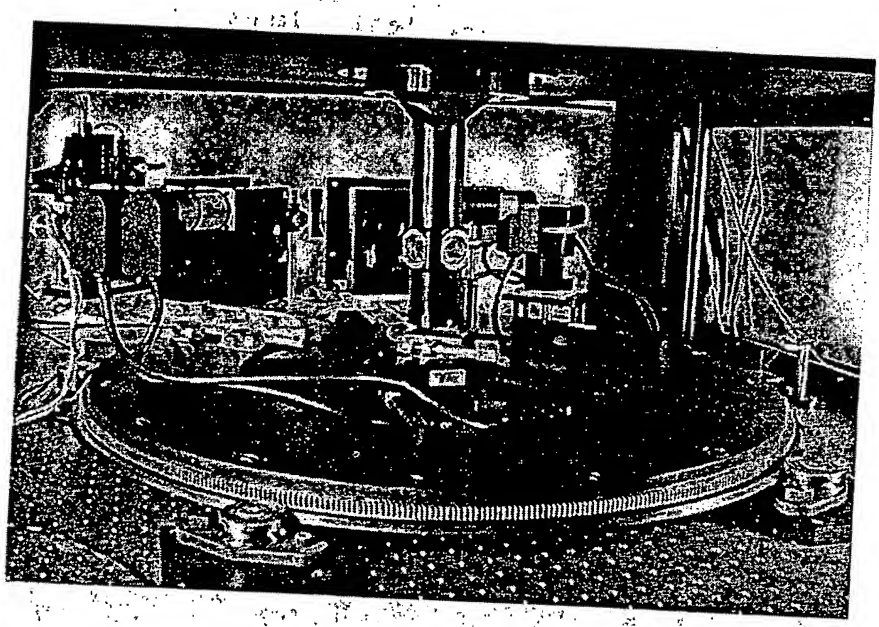

Figure 8. Photograph of a goniometer system used for absolute and relative reflectance and transmittance of samples a temperatures ranging from 10 K through 600 K. Vertically mounted rotation stages on the fixed input rail and the movabl detector rail are used to hold and manipulate polarizers and retarders for the characterization of the polarization properties o samples and components.

The input beam to the goniometer can be adjusted from f/18 to ~f/80. Using the cryostat, the sample temperature can be varied from 10 K to 600 K. And with polarization elements, the full Mueller Matrix of a sample can be characterized. For the comparison measurements described here, no polarizers were used and the beam was adjusted 8° incidence with f/20.

Two samples were measured on both systems: a protected Ag mirror and an anti-reflection-coated sapphire window. The measured reflectance of the Ag mirror is shown in Figure 9. These measurements were made prior to installation of a system purge enclosure. This results in CO_2 and H_2O absorption structure apparent in both spectra. For the goniometer measurements, the Ag mirror was mounted in a cryostat and measured under vacuum. Alignment of the beam for reflectance and transmittance was achieved through careful adjustment of the sample tilt and detector position. Nevertheless, the dominant source of error for the goniometer measurements remains the misalignment of the reflected and transmitted light on the detector. In addition, changes in path length through the CaF_2 windows of the cryostat result in additional error at longer wavelengths (i.e. beyond 9 μm) where the windows begin to absorb. The estimated expanded uncertainty (approx. two standard deviations) for the goniometer system in the regions outside the atmospheric absorption is approximately 0.015. The estimated expanded uncertainty (coverage factor, k = 2) of the sphere measurement for the same spectral regions is 0.003.

With the addition of a purge enclosure for both systems, made prior to the sapphire comparison measurements, these uncertainty levels apply to the entire spectral region.

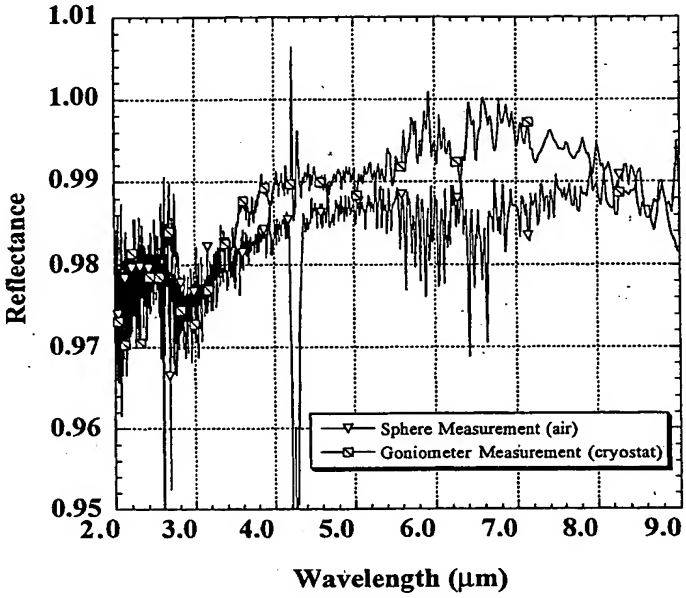

Figure 9. Direct comparison of integrating sphere and goniometer absolute reflectance measurements of a protected Ag mirror in the infrared spectral region. Structures from 2.6 μm to 3.0 μm, at 4.2 μm and from 5.6 μm to 7.0 μm are due to atmospheric absorption effects not related to the Ag mirror.

A sapphire infared window was also characterized using both the integrating sphere and goniometer systems. Both the reflectance and transmittance were characterized on both systems. The results are shown in Figure 10. A purge enclosure was in operation for these measurements. The sapphire window has an anti-reflection coating optimized for 4 μm wavelength. Due to the coating, the transmittance and reflectance in Figure 10 vary considerably from uncoated sapphire values. The agreement between the sphere and goniometer measurement results appears good. A closer look at the results is shown in Figure 11.

For each system the absorptance is calculated from the transmittance and reflectance data shown in Figure 10. The absorptance values nearly span the complete range from 0 to 1. To compare the two method's results, the difference between the two absorptance spectra is plotted in Figure 11. Two primary features stand out. The feature at 8 μm is not understood at present, but is under study. The sinusoidal variation for shorter wavelengths is attributed in part to the angular dependence of the anti-reflection coating. Samples with a strong sensitivity to angle of incidence will naturally have larger uncertainties associated with their measurement. Both the difference in the beam geometries of the two systems, and the slight variation in angle of incidence for the transmittance and reflectance sample measurements of the two systems can result in larger 'errors' in the calculation of absorptance. More accurate angle of incidence alignment in both vertical and horizontal planes, combined with corrections for the difference in input beam geometries is expected to reduce the size of the variations seen in Figure 11.

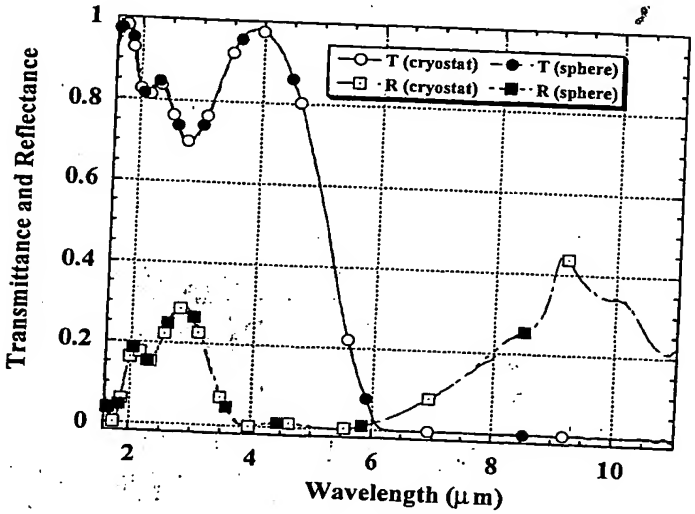

Figure 10. Absolute reflectance and transmittance of a coated sapphire window, as measured by integrating sphere and goniometer (with cryostat) systems.

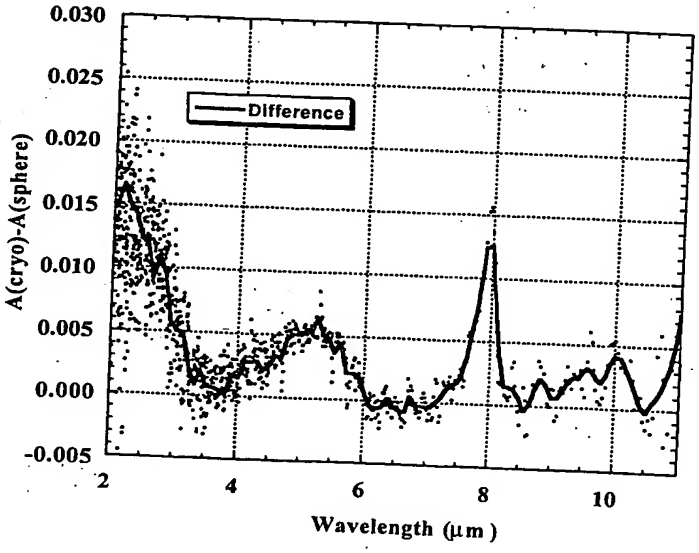

Figure 11. Difference in the absorptance of a coated sapphire window, as indirectly measured by the goniometer and sphere systems.

5. CONCLUSIONS

Four methods for the absolute measurement of reflectance have been described and evaluated in terms of the characterization of transmissive materials. Certainly these materials present more difficulty for accurate measurement than opaque materials do. A qualitative comparison of the four methods has been presented along with a quantitative comparison of infrared implementations of two of the methods: the integrating sphere and goniometer methods. In most cases alignment errors dominate the measurement uncertainty. Where feasible, integrating spheres can be used to significantly reduce these errors, as in the case of the integrating sphere method. The incorporation of transmittance measurement under the same beam geometry conditions is an important tool in the evaluation of the reflectance results and measurement uncertainties.

Two methods for absolute reflectance described in this paper have been implemented on a FT spectrophotometer for the infrared spectral range. In the direct comparison of these two methods using two types of samples, the agreement between the infrared integrating sphere and goniometer systems is reasonably good and within the estimated levels of uncertainty. The planned addition of larger area, more spatially uniform detectors or averaging spheres should result in improved performance of the goniometer system.

6. REFERENCES

[1] L. M. Hanssen, "Integrating sphere system for absolute measurement of infrared transmittance, reflectance and absorptance of specular samples," submitted to Applied Optics (1998).

[2] J. Strong, *Procedures in Experimental Physics*, p. 376, Prentice-Hall, New York, (1938).

[3] N. Ooba, W. Erb, et al, *Absolute Methods for Reflectance Measurements*, Publication No. 44 (TC-2.3), CIE, Vienna (1979).

[4] A. W. Springsteen, "Reflectance spectroscopy : an overview of classification and techniques," in A. W. Springsteen and J. Workman (ed.) *Applied Spectroscopy: a Compact Reference for Practitioners*, pp. 193-224, Academic Press, New York, (1998).

[5] T. M. Wang, K. L. Eckerle, and J. J. Hsia, "Absolute specular reflectometer with an autocollimator telescope and auxiliary mirrors," NIST Technical Note 1280, U.S. Gov't Printing Office, Washington, 1990.

[6] F. J. J. Clarke, "Infrared regular reflectance standards from NPL," Proc. SPIE **2776**, 184-195 (1997).

[7] L. M. Hanssen and S. A. Kaplan, "Infrared diffuse reflectance instrumentation and standards at NIST," *Proceedings of the 3rd Oxford Conference on Optical Spectrometry*, Egham, United Kingdom, June 28 – July 2, 1998, Mikrochimica Acta, in press (1998).

[8] K. A. Snail and L. M. Hanssen, "Integrating sphere designs with isotropic throughput", Applied Optics **28** no. 10, 1793-1799 (1989).

[9] L. M. Hanssen and S. A. Kaplan, "Problems posed by scattering transmissive materials for accurate transmittance and reflectance measurements," in *Optical Diagnostic Methods for Transmissive Inorganic Materials*, Proc. SPIE **3425** in press (1998).

[10] S. A. Kaplan and L. M. Hanssen, "Infrared regular reflectance instrumentation and standards at NIST," *Proceedings of the 3rd Oxford Conference on Optical Spectrometry*, Egham, United Kingdom, June 28 – July 2, 1998, Mikrochimica Acta, in press (1998).

[11] E. D. Palik, ed., *Handbook of Optical Constants of Solids*, p. 552 –570, Academic Press, New York (1985).

[12] D. B. Chenault, K. A. Snail, and L. M. Hanssen, "Improved integrating sphere throughput with a lens and nonimaging concentrator," Applied Optics **34**, no. 34, 7959-7964 (1995).